Dual-Frequency and Broad-Band Antennas with Stacked Quarter Wavelength Elements

Lakhdar Zaïd, Georges Kossiavas, Jean-Yves Dauvignac, Josiane Cazajous, and Albert Papiernik

***Abstract*—Original lightweight, low-cost, and compact air-filled planar antennas with short-circuited elements, fed by coaxial probe, for dual-frequency (S-antenna) and wide-band applications (E-antenna) are investigated. The two-band frequency antenna is formed of two stacked quarter-wavelength elements, short-circuited along diametrically opposed planes. This structure offers two modes with different radiation characteristics. The ratio between the two frequencies can be closely controlled within a range varying from 1.3–2. A bandwidth of 30% for a VSWR < 2 is demonstrated using two stacked quarter-wavelength elements short-circuited along the same plane. Numerical simulation results are compared with experiments and a very good agreement is observed. Radiation patterns and input impedance of both structures are measured and the effects of various physical parameters are presented.**

***Index Terms*— Broad-band antennas, dual frequency antennas, microstrip antennas, quarter-wavelength elements, stacked patches.**

I. Introduction

MOBILE communications systems have improved mobility very considerably, but the antenna still remains a bulky element, and attempts are continually being made to reduce its size. However, reducing antenna dimensions results in a decrease of bandwidth [1] and this effect is independent of the technology used. Moreover, microstrip patch antennas have inherently narrow bandwidth [2] and in many systems, it is necessary to design large bandwidth structures. On the other hand, in dual-frequency applications it is very attractive to be able to cover the transmission and reception bands simultaneously with one antenna.

In order to obtain a dual-band [3] or a broad-band microstrip antenna [4], one solution is to use only one element by adding shorting pins and/or etched slots on the patch. More bandwidth enhancement can be achieved by two main methods. The first involves the use of an electrically thick element [5] and the second requires a reduction of substrate permittivity. In fact, the increase of substrate thickness has the effect of reducing the radiation Q factor and thus improving the bandwidth. But a substrate thickness improvement causes a lack of compactness, a higher cross-polarization level and increases excitation of surface waves [6] that deteriorate the quality of the radiation patterns. Moreover, a broad-band impedance-matching network can be used as a method for bandwidth improvement of microstrip antennas [7]. Other configurations with enhanced bandwidth have already been investigated. Thus, the input impedance bandwidth of a microstrip antenna can be improved by using the effect of mutual coupling between stacked [8], [9] or juxtaposed [10] microstrip patches and sometimes the two methods are combined [11]. The juxtaposed configuration involves placing elements near each other, coupled to the radiating [12] or nonradiating edge [13] but the drawback of this kind of arrangement is that it results in a wider structure [14].

The purpose of this study is to investigate the input impedance, the resonant frequency, the current density maps on the surface of each resonator and far field radiation patterns of these two structures. The different radiating elements considered are end-shorted along one edge. An end-shorted element presents the advantage of the smallest size with a length of $\lambda/4$, a broad beamwidth and a bandwidth which is reduced compared with a half element. The dual frequency S-antenna is made using two stacked quarter-wavelength elements short-circuited along diametrically opposed planes, whereas the E-antenna is composed of two stacked quarter-wavelength elements short-circuited along the same plane. Numerical simulation results have been compared with experiments and a very good agreement is observed. The effects of several physical parameters are presented and discussed.

II. Numerical Simulation

The Systems Radiated Three-Dimensional (SR3D) simulation tool which has been developed by France Telecom/CNET [15], [16] was used to study both antennas. It is based on a surface finite-element method that solves the electromagnetic field integral equations in the harmonic domain. The code requires all the surfaces of the geometry (patches, ground plane, coaxial probe) to be divided into triangular cells. When the electric and magnetic current densities are known on all surfaces of the antenna, electric fields can be calculated anywhere else. In this way, the input impedance of the antenna, the current densities map on each resonator and, similarly, near and far-field radiation can all be determined. Moreover, the thickness of the metal layers is also taken into account. The reflection coefficient is computed in the cross section of the coaxial probe using guided mode excitation [15]. A coaxial probe is used to feed each antenna.

Manuscript received December 2, 1997; revised January 5, 1999. This work was supported by France Telecom/CNET.

The authors are with the Laboratoire d'Electronique, Antennes et Télécommunications, Université de Nice-Sophia Antipolis, CNRS UPRESA 6071, Valbonne, 06560 France.

Publisher Item Identifier S 0018-926X(99)04771-7.

0018–926X/99$10.00 © 1999 IEEE

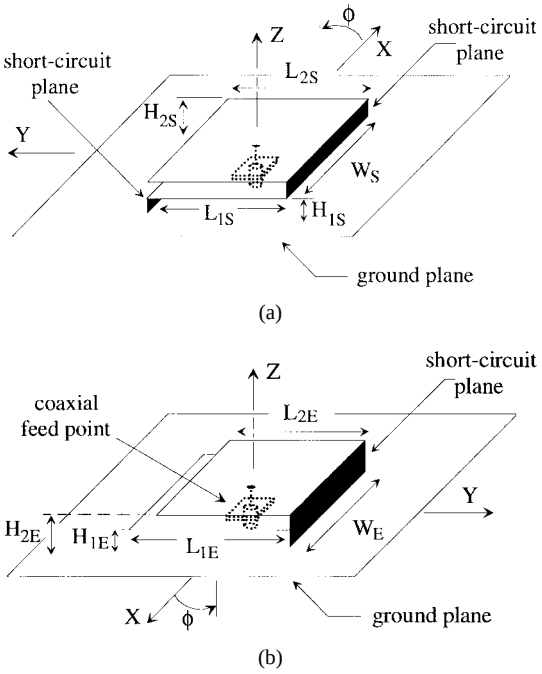

Fig. 1. Geometry of (a) S-antenna and (b)E-antenna . $H_{1E} = 6.8$ mm, $H_{2E} = 11.6$ mm, $W_E = 35$ mm, $L_{1E} = 35$ mm, $L_{2E} = 25$ mm; $H_{1S} = 8$ mm, $H_{2S} = 13.5$ mm, $W_S = 35$ mm, $L_{1S} = 35$ mm, $L_{2S} = 35$ mm.

III. Geometry of Antennas

The dual-frequency and broad-band antennas are shown in Fig. 1(a) and (b), respectively. Both structures are realized with rectangular 0.3-mm copper sheets on air substrate to provide the largest bandwidth for a total height $H_{2(S,E)}$ mm. The main geometrical difference between the two antennas lies in the short-circuit planes. The dual-frequency S-antenna [Fig. 1(a)] is designed with two stacked opposed quarter-wavelength elements and is obtained entirely by folding. The E-antenna [Fig. 1(b)] is manufactured in several steps. First, the upper resonator is folded at a right angle, then the lower element is soldered against the vertical short plane and finally the structure is soldered onto a 100 × 100 mm ground plane which is identical for each geometry. The widths of both structures are equal ($W_S = W_E = 35$ mm). The lower patches are fed by a 50 Ω coaxial probe at the midpoint of the longer side $W_{S,E}$, at a distance of 21 mm and 18 mm from the short-circuit plane for the S-antenna and the E-antenna, respectively. The diameter of the inner conductor was chosen slightly larger (1.2 mm) to minimize inductance through the first layers $H_{1(S,E)}$. The location of the feeding probe is symmetric with respect to the y axis.

IV. Dual-Frequency S-Antenna

Fig. 1(a) shows a perspective view of the dual-frequency antenna. The S-antenna consists of two opposite stacked quarter-wavelength elements. The resonant frequency and input impedance were measured with an HP8720B network analyzer and the radiation pattern measurements were carried out with the antenna under test placed inside an anechoic chamber. The simulated coaxial probe was designed to have 50 Ω characteristic impedance. The simulated resonant frequencies

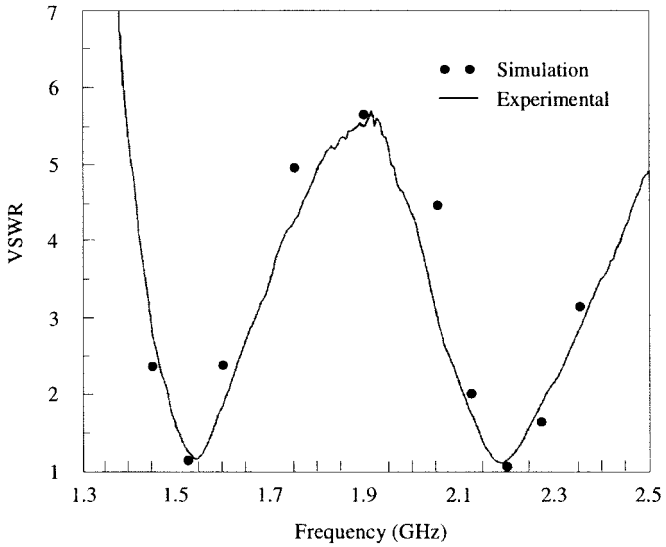

Fig. 2. Measured and simulated VSWR versus frequency of S-antenna.

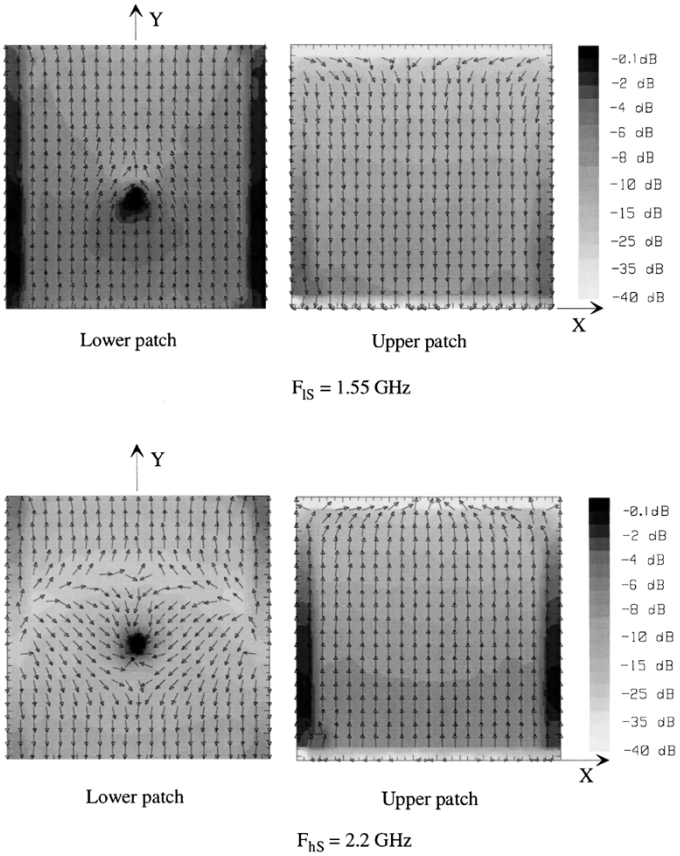

Fig. 3. Current density maps of S-antenna at both operating frequencies.

are compared to the measured and theoretical data (Fig. 2). We obtained two working frequency bands centered at $F_{lS} = 1.55$ GHz and $F_{hS} = 2.2$ GHz with a bandwidth of eight and 10% for a VSWR better than two, respectively. A good agreement is observed between simulated and experimental results over the broad band and even near the lower levels of VSWR.

According to the electric current density maps of metallic layers (Fig. 3), it follows that two different current distri-

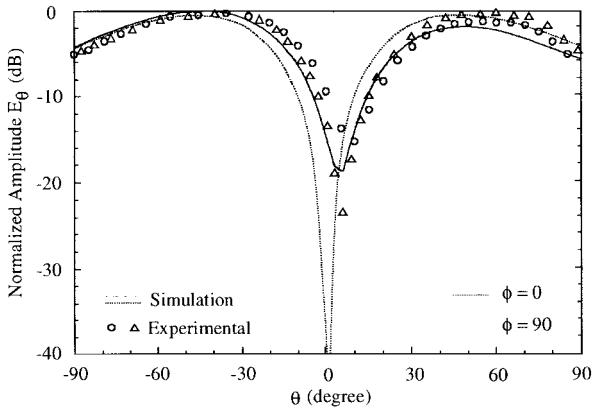

Fig. 4. S-antenna: Measured and simulated radiation patterns at $F_{lS} = 1.55$ GHz.

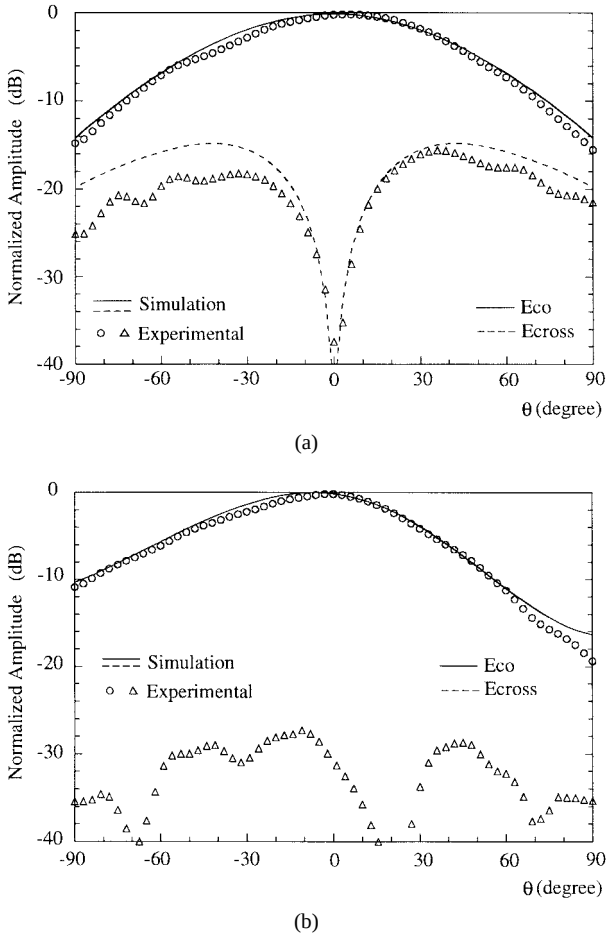

Fig. 5. S-antenna: Measured and simulated radiation patterns at $F_{hS} = 2.2$ GHz. (a) Plane $\phi = 0$. (b) Plane $\phi = 90$.

butions are observed over each resonator. This phenomenon affects the radiation patterns, also giving different radiation properties at the two working bands. The radiation patterns in plane $\phi = 0$ and 90° of the S-antenna are presented for each matched frequency band in Figs. 4 and 5.

Therefore, the contribution of the current distribution on the upper and lower patches shows that the current density vectors on the metallic layers are in phase opposition at the lower frequency band (Fig. 3). Consequently, the level of the

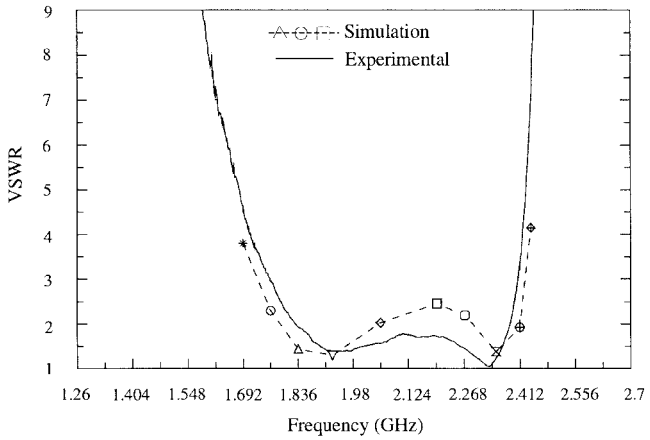

Fig. 6. Measured and simulated VSWR versus frequency of E-antenna.

TABLE I
INPUT IMPEDANCE BANDWIDTH VERSUS HEIGHT OF THE E-ANTENNA

H_{1E}	H_{2E}	Bandwidth (VSWR<2)
3 mm	5 mm	15.4 %
3 mm	5.5 mm	18.6 %
4 mm	7 mm	23 %
5.5 mm	10.5 mm	29.5 %

E_θ component in the broadside direction is expected to be low. Thus a beam shift is observed in principal planes where the main beam directions of E_θ are obtained for $\theta = \pm 45°$ for scan angles $\phi = 0$ and 90° (Fig. 4). The directivity gain concerning the lower frequency band ($F_{lS} = 1.55$ GHz) is also computed in the maximum direction and gives 2.5 dB, and we have measured in our anechoic chamber a gain of 1.5 dB.

With regard to the upper band, the longitudinal current distributions are in phase opposition on the lower metallic layer and especially near the edges (Fig. 3). The current vectors are oriented along the same direction on the upper metallic layer which gives a symmetrical radiation pattern and a linear polarization along the y axis with a -3-dB beamwidth of about 75° for $\phi = 90°$ (Fig. 5). In the same way, the computed directivity gain is 8 dB in the maximum direction at $f = 2.2$ GHz and the measured gain is 7.6 dB for this frequency.

V. BROAD-BAND E-ANTENNA

A global view of the E-antenna geometry is presented in Fig. 1(b). For this structure a 10 dB impedance bandwidth of 25% is achieved. A good agreement is observed between simulated and experimental results (Fig. 6). Thus, this stacked configuration gives two resonance modes allowing a wider band than with one quarter-wavelength element, for the same thickness. Table I shows the bandwidth of the E-antenna for different heights of radiating elements. In this configuration, the two square layers were taken identical with $L_{1E} = L_{2E} = 35$ mm. It is seen that the bandwidth can be varied from 15.4% for 5 mm total height to 30% with 10.5 mm.

The far-field radiation patterns in the two principal planes were also computed for $F = 2.35$ GHz (Fig. 7) and the agreement with the experiment is good, principally for E_{co} and E_{cross} in scan angle $\phi = 0$ degree. Moreover, the radiation

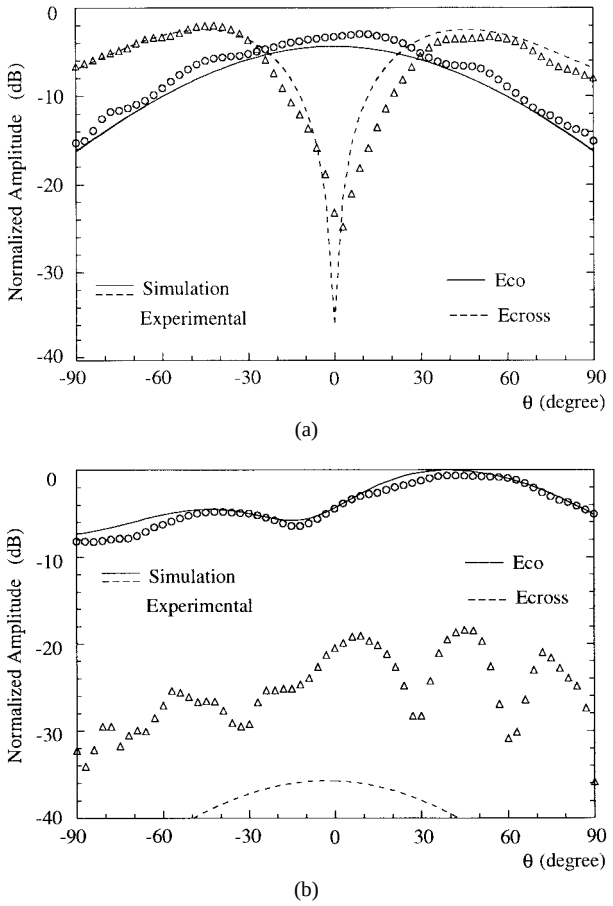

Fig. 7. E-antenna: Measured and simulated radiation patterns at $F = 2.35$ GHz. (a) Plane $\phi = 0$. (b) Plane $\phi = 90$.

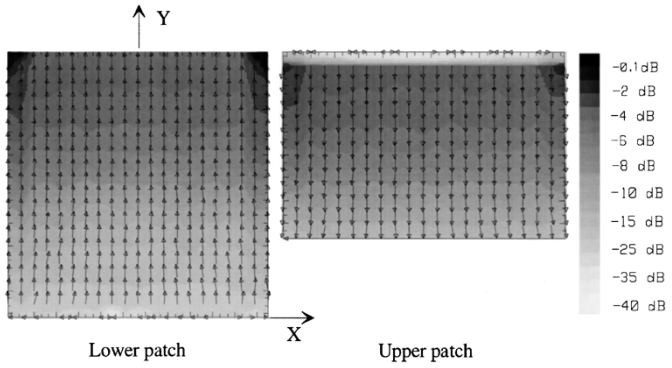

Fig. 8. Current density maps of E-antenna for each resonator ($F = 2.35$ GHz).

patterns have the same characteristics (linear polarization along y axis) over the broad band. It should be noted that there is a beam squint of about 45° in $\phi = 90°$ plane that is explained by the magnitude of current distributions on the metallic layers which are strong near the short-circuited edges of the superposed radiating elements (Fig. 8).

We can note a high level of cross polarization of -3 dB for $\theta = 45°$ in the plane $\phi = 0°$ and $180°$. First, it is not in the direction of the maximum beam. This result was expected in view of the small dimensions of the antenna with respect to the wavelength. With this kind of antenna (E and S), a high purity of polarization as with a horn antenna or classical

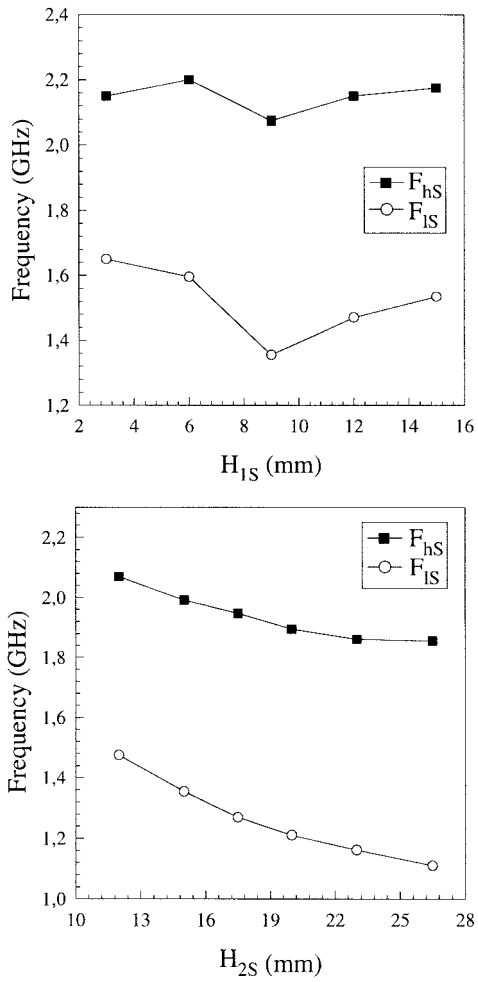

Fig. 9. S-antenna: Variation of both operating frequencies against height. Other parameters are identical to the ones of Fig. 1.

microstrip patch can never be obtained. These antennas can be classified in the "blurred polarization" family.

This high level of cross polarization might limit the use of the E antenna in the direction $25° < \theta < 80°$ for $\phi = 0°$ and $180°$. But a low level of cross polarization ($E_{\text{cross}} < -20$ dB) is obtained in the plane $\phi = 90$ (symmetric plane) and in the direction of the maximum beam.

The computed directivity gain in the main beam direction ($\theta = 45°$) varies with frequency from 4 dB. We have measured a maximum gain of 5.5 dB for the upper frequencies of the bandwidth and it decreases for the low frequencies of the bandwidth.

VI. Parameter Study

In this section, an experimental study of the main parameters of these structures was carried out and the results obtained are represented in terms of frequency curves (S-antenna) and real part of the input impedance (E-antenna). The resonance frequency is defined as the maximum of the input resistance.

The S-antenna can easily be matched at two frequencies using all the main parameters. Moreover, the position of the feeding point strongly affects the input impedance level. In fact, the latter decreases as the coaxial probe feed moves

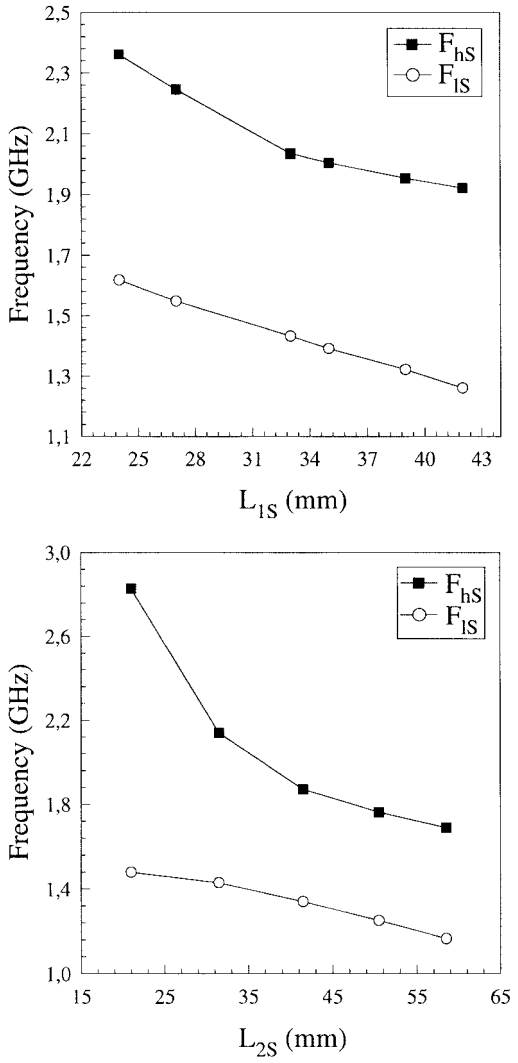

Fig. 10. S-antenna: Variation of both operating frequencies against length. Other parameters are identical to the ones of Fig. 1.

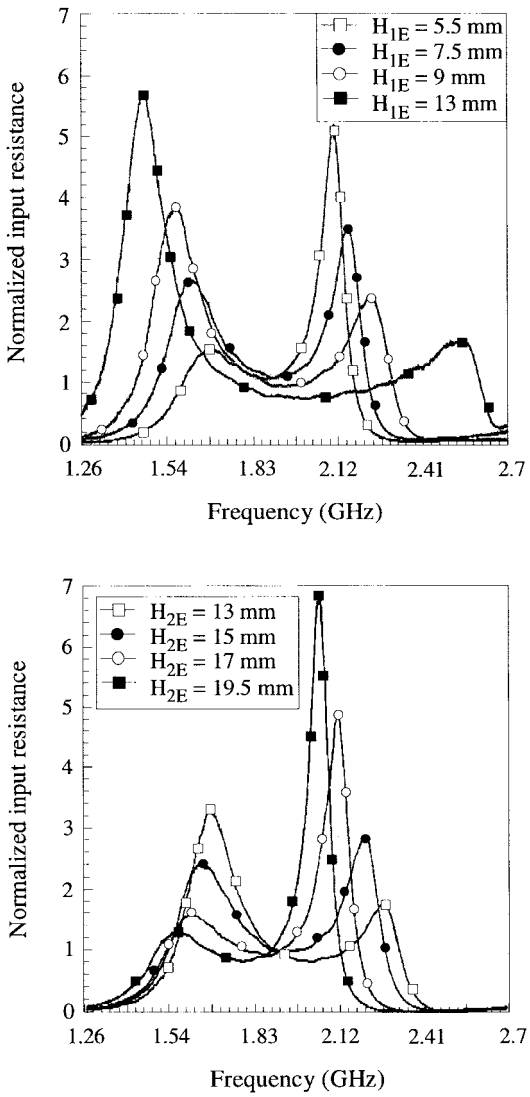

Fig. 11. Real parts of the input impedance of E-antenna as a function of height patches. Other parameters are identical to the ones Fig. 1.

toward the shorting plane. For antennas having two or more discrete working bands, it is important to know the effects of physical parameters on resonant frequencies and especially on the frequency ratio $(F_{rS} = F_{hS}/F_{lS})$. Similar variations can be observed for frequency curves (Fig. 9) when the height of the lower patch H_{1S} increases from 3–15 mm. A minimum point frequency is observed simultaneously for values of H_{1S} close to 9 mm. The parameter H_{2S} weakly influences the frequency ratio. This ratio varies from 1.4–1.7 with a decrease of both frequencies when H_{2S} improves. As regards the lower patch length, the two resonant frequencies of the antenna are found to decrease with an increase of L_{1S} (Fig. 10). It is also noted that the lower operating frequency varies linearly with presented values of L_{1S}. Moreover, the variation between both frequencies is almost constant. The two resonant frequencies can be very close $(F_{rS} = 1.4)$ when the upper patch length (L_{2S}) becomes high. This behavior is different for small values of L_{2S} for which a large frequency ratio around $F_{rS} = 2$ is obtained. Consequently, the upper element length is the physical parameter that greatly influences the ratio between the two operating frequencies. For values of L_{2S} varying from 21 to 58 mm, the lower frequency changes slightly (300 MHz), whereas the upper frequency range is four times as large.

For the first E-antenna curve, the total height $H_{2E} = 11.6$ mm is kept constant for different values of H_{1E}. It is seen that the real normalized part of the input impedance seems to be proportional to H_{1E} for values of $H_{1E} = 5.5$, 7.5, 9, 13 mm (Fig. 11). The frequency ratio $(F_{rE} = F_{hE}/F_{lE})$ increases with H_{1E} and varies from 1.2 to 1.8. For high values of F_{rE} the broad-band aspect is not maintained. With the variation of the electrical thickness H_{2E} (E-antenna) for a given value $H_{1E} = 6.8$ mm, we can notice a low global decrease of resonant frequencies with a slight influence on the frequency ratio (Fig. 11). In this case, the upper resonant peaks for high values of H_{2E} (17, 19.5 mm) become too important and input impedance matching remains difficult to obtain.

The real part of input impedance for different lengths of the coupled resonators is plotted in Fig. 12. As the length of the lower element (L_{1E}) increases from 29 to 38 mm, the resonant frequencies shift down whereas the ratio between them improves slightly. The lower peak magnitude of the

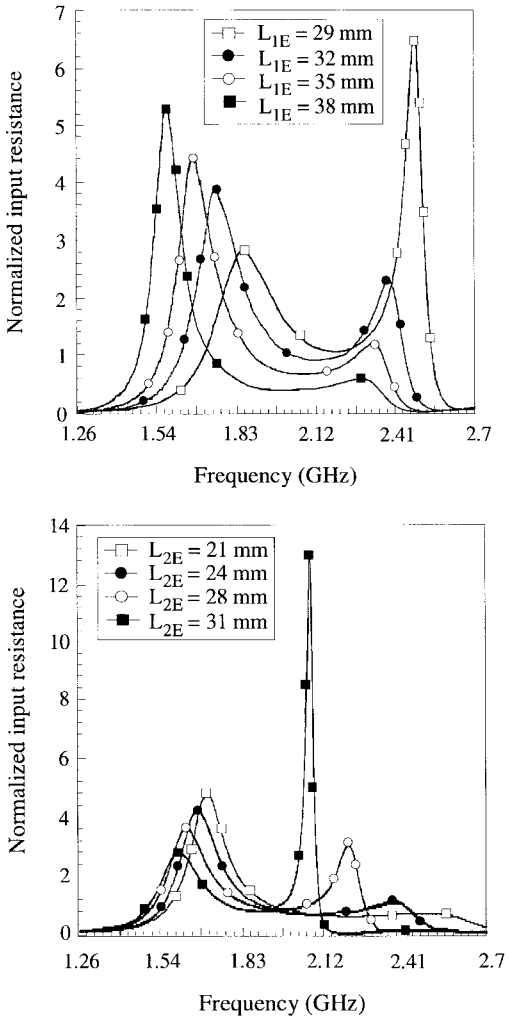

Fig. 12. Real parts of the input impedance of E-antenna as a function of length patches. Other parameters are identical to the ones Fig. 1.

real part increases with L_{1E} whereas the upper magnitude peak decreases. The higher frequency is more influenced by the upper resonator length L_{2E}, while its working range is three times greater than that obtained with the lower length. When the upper length resonator varies from 21 to 31 mm, the higher frequency changes from 2.5 to 2.1 GHz and the lower decreases slightly from 1.7 to 1.6 GHz. Moreover, for range values greater than 31 mm, the resonance peak at the higher frequency increases to higher values (650 Ω), while that at the lower frequency decreases. The frequency ratio varies from 1.45 down to 1.3 when length L_{2E} increases.

VII. Conclusion

Original compact antennas having dual-frequency and large bandwidth operation have been presented. The antennas excited by a coaxial probe use stacked quarter-wavelength elements placed along diametrically opposed planes (S-antenna) and along the same plane (E-antenna). Experimental study of the principal physical parameters of both structures was carried out. Moreover, for better simulation results, the thickness of sheet copper was taken into account. The predicted resonant frequencies are very close to the measured values. The S-antenna provides two discrete bands with a frequency ratio that can be adjusted from 1.3 to 2. The resonant modes of the operating bands give different radiation patterns. The lower working frequency provides a beam for $\theta = \pm 45°$ and a broadside radiation pattern is obtained for the upper operating frequency. The broad-band E-antenna provides an optimum bandwidth of around 30% using thicker elements with a size of approximately quarter wavelength. The radiation pattern has the same characteristics over the broad band, with a shift of 45 with regard to the zenith in the E-plane. These original stacked configurations should find use in applications where wider impedance bandwidth, dual-band operation and diversity of radiation properties are needed.

Acknowledgment

The authors are very grateful to CNET La Turbie for providing the computer resources (SR3D) used to perform antenna simulations.

References

[1] H. A. Wheeler, "Small antennas," *IEEE Trans. Antennas Propagat.*, vol. AP-23, pp. 462–469, July 1975.
[2] K. R. Carver and J. W. Mink, "Microstrip antenna technology," *IEEE Trans. Antennas Propagat.*, vol. AP-29, pp. 2–24, Jan. 1981.
[3] B. F. Wang and Y. T. Lo, "Microstrip antennas for dual-frequency operation," *IEEE Trans. Antennas Propagat.*, vol. AP-32, pp. 938–943, Sept. 1984.
[4] T. Huynh and K. F. Lee, "Single-layer single-patch wideband microstrip antenna," *Electron. Lett.*, vol. 31, no. 16, pp. 1310–1312, Aug. 1995.
[5] E. Chang, S.A. Long, and W. F. Richards, "An experimental investigation of electrically thick rectangular microstrip antennas," *IEEE Trans. Antennas Propagat.*, vol. AP-34, pp. 767–772, June 1986.
[6] D. R. Jackson, J. T. Williams, A. K. Bhattacharyya, R. L. Smith, S. J. Buchheit, and S. A. Long, "Microstrip patch designs that do not excite surface waves," *IEEE Trans. Antennas Propagat.*, vol. 41, pp. 1026–1037, Aug. 1993.
[7] H. F. Pues and A. R. van de Capelle, "An impedance-matching technique for increasing the bandwidth of microstrip antennas," *IEEE Trans. Antennas Propagat.*, vol. 37, pp. 1345–1353, Nov. 1989.
[8] F. Croq, G. Kossiavas, and A. Papiernik, "Stacked resonators for bandwidth enhancement: A comparison of two feeding techniques," *Proc. Inst. Elect. Eng.*, pt. H, vol. 140, no. 4, pp. 303–307, Aug. 1993.
[9] H. R. Hassani and D. Mirshekar-Syahkal, "Study of electromagnetically coupled stacked rectangular patch antennas," *Proc. Inst. Elect. Eng. Microw. Antennas Propagat.*, vol. 142, no. 1, pp. 7–13, Feb. 1995.
[10] F. Croq and D. M. Pozar, "Multifrequency operation of microstrip antennas using aperture coupled parallel resonators," *IEEE Trans. Antennas Propagat.*, vol. 40, pp. 1367–1373, Nov. 1992.
[11] H. Legay and L. Shafai, "New stacked microstrip antenna with large bandwidth and high gain," *Proc. Inst. Elect. Eng. Microw. Antennas Propag.*, vol. 141, no. 3, pp. 199–204, June 1994.
[12] G. Kumar and K. C. Gupta, "Broad-band microstrip antennas using additional resonators gap-coupled to the radiating edges," *IEEE Trans. Antennas Propagat.*, vol. AP-32, pp. 1375–1379, Dec. 1984.
[13] C. K. Aanadan, P. Mohanan, and K. G. Nair, "Broad-band gap coupled microstrip antenna," *IEEE Trans. Antennas Propagat.*, vol. 38, pp. 1581–1586, Nov. 1992.
[14] Y. K. Cho, G. H. Son, G. S. Chae, L. H. Yun, and J. P. Hong, "Improved analysis method for broadband rectangular microstrip antenna geometry using E-plane gap coupling," *Electron. Lett.*, vol. 29, no. 22, pp. 1907–1908, Oct. 1993.
[15] P. Ratajczak, P. Brachat, and J. L. Guiraud, "Rigorous analysis of three-dimensional structures incorporating dielectrics," *IEEE Trans. Antennas Propagat.*, vol. 42, pp. 1077–1088, Aug. 1994.
[16] P. Brachat, C. Dedeban, Ph. Ratajczak, and Th. Bousquet, "Analyze de structures tridimensionnelles inhomogènes complexes," in *Proc. JINA'96, Int. Conf.*, Nov. 1996, pp. 425–438.

Lakhdar Zaïd was born in Chelghoum-laïd, Algeria, on November 5, 1968. He received the D.E.A degree in propagation, detection and communications from the University of Toulon (France) in 1995 and the Ph.D. degree in electrical engineering from the University of Nice-Sophia Antipolis (France) in 1998.

His research interests are the reduction size of antennas for mobile and indoor communications systems.

Georges Kossiavas received the Ph.D. degree in electronics from the University of Limoges, France in 1981.

Since then he has been an Assistant Professor at the Ecole Supérieure d'Ingénieurs de Nice, Sophia-Antipolis (ESINSA), University of Nice, Sophia-Antipolis, France. He works also at the Laboratoire d'Electronique Antennes et Télécommunications (LEAT) CNRS-UPRESA 6071, Sophia-Antipolis, France. His research interests include microstrip antennas, especially large bandwidth and high-purity polarization radiating elements and compact microstrip antennas for the mobile communications systems.

Jean-Yves Dauvignac was born in Sisteron, France, on December 22, 1965. He received the M.S. degree in telecommunications of the University of Toulon, France, in 1987, the D.E.A. degree in microwave communications and signal processing from the University of Nice-Sophia Antipolis (UNSA), France, and the Ph.D. degree in electrical engineering from the UNSA in 1993.

Since 1993, has been an Assistant Professor at the Telecommunications and Networks Department of the Institute of Technology at the UNSA. He is currently a Research Scientist at the Electronic Laboratory of the UNSA. His current research interest includes numerical methods in electromagnetics, especially the finite-element method for antenna modeling and inverse method for microwave imaging.

Dr. Dauvignac is a member of the steering and organization committees of the JINA International Symposium on Antennas.

Josiane Cazajous received the Dipl.Eng. degree from Ecole Polytechnique Féminine, Sceaux, France, in 1992, and the D. E. A. degree in propagation, remote sensing, and telecommunications from the University of Nice, Sophia Antipolis, France, in 1994.

From 1994 to 1996, she researched miniaturized active printed antenna concepts for mobile communications, at the Laboratoire d'Electronique Antennes et Télécommunications (LEAT) CNRS-UPRESA 6071, Sophia-Antipolis, France. Since 1996 she has been a Study Engineer at the Alcatel Space Industries Antenna Department, Toulouse, France, on the Stentor Ku-band planar active antenna for a telecommunications satelite program.

Albert Papiernik received the Agrégation de Sciences Physiques degree in 1964 from the Ecole Normale Supérieure de Saint-Cloud and Doctorat-ès-Sciences degree in 1969 from Orsay University.

From 1964 to 1970, he was a Researcher at the Centre National de la Recherche Scientifique (CNRS). From 1970 to 1984 he was a professor of electrical engineering at Limoges University. Currently, he is Professor at the University of Nice, Sophia-Antipolis. His research interests include microstrip antennas. He is studying large bandwidth and high-purity polarization radiating elements by using the integral equations in spectral domain or transmission-line matrix method.